Laminar mixing and chaotic mixing in several cavity flows

By W.-L. CHIEN,
Department of Chemical Engineering, University of Massachusetts, Amherst, MA 01003, USA
H. RISING
Department of Mathematics, University of Massachusetts, Amherst, MA 01003, USA
AND J. M. OTTINO
Department of Chemical Engineering, University of Massachusetts, Amherst, MA 01003, USA

(Received 19 August 1985 and in revised form 15 January 1986)

The objective of this work is an experimental study of laminar mixing in several kinds of two-dimensional cavity flows by means of material line and blob deformation in a new experimental system consisting of two sets of roller pairs connected by belts. The apparatus can be adjusted to produce a range of aspect ratios (0.067–10), Reynolds numbers (0.1–100), and various kinds of flow fields with one or two moving boundaries. Flow visualization is conducted by marking underneath the free surface of the flow with a tracer solution of low diffusivity and of approximately the same density and viscosity as the flowing fluid. The effects of the initial location of the material blob, relative motion of the two bands, and minor changes in the geometry of the flow region are investigated experimentally.

The alternate periodic motion of two bands in a cavity flow is an example of a laminar flow which might lead to chaotic mixing. The governing parameter is the dimensionless frequency of oscillation of the walls f which, under the proper conditions, is able to produce horseshoe functions of various types. The deformation of blobs is central to the understanding of mixing and can be studied to identify horseshoe functions. It is found that the efficiency of mixing depends strongly on the value of f and that there exists an optimal value of f that produces the best mixing in a given time.

1. Introduction

The calculation of velocity fields and mixing in cavity flows (see figure 1*a*) has theoretical and practical importance. Most studies have focused on streamline visualization at high Reynolds numbers (Burggraf 1966; Pan & Acrivos 1967; Greenspan 1974; Nallasamy & Prasad 1977; Vahl Davis & Mallinson 1976; Winters & Cliffe 1979; Schreiber & Keller 1983*a*, *b*; Peyret & Taylor 1983).

Studies of mixing in low-Reynolds-number flows are much more scarce in spite of its practical importance. The simplest cavity flow, i.e. Type I (figure 1*a*), corresponds to the cross-section of one of the most common mixing devices in polymer processing: the single screw extruder (Middleman 1977). Bigg & Middleman (1974) have studied the mixing of two fluids with different viscosities in the standard cavity flow (figure 1*a*) by means of the Marker and Cell technique (MAC) (Harlow & Amsden 1970). Experiments were conducted on a box of fixed aspect ratio with a moving upper wall; only one initial mixing configuration (a horizontal interface at $y = \frac{1}{2}H$) was studied.

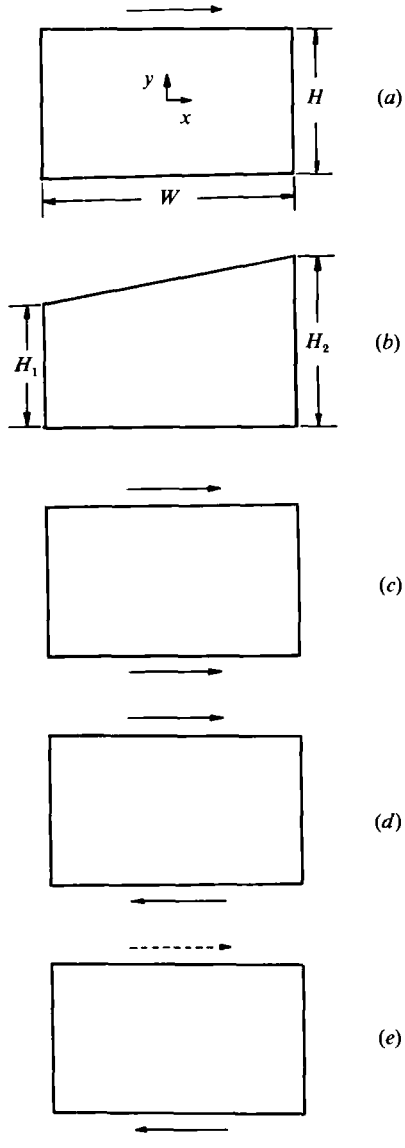

FIGURE 1. Various kinds of cavity flows. (*a*) standard cavity flow or Type I cavity flow; (*b*) one-side tilted cavity flow; (*c*) Type II cavity flow; (*d*) Type III cavity flow; (*e*) alternate periodic cavity flow.

Given the dimensions of the box (height 7.95 cm, width 15.2 cm, depth 7.6 cm) secondary flows should not be ruled out. Other mixing studies of Type I cavity flows are reviewed by Chella & Ottino (1985*a*).

The objective of the first part of this work is to present a new apparatus that allows one to create a greater variety of two-dimensional low-Reynolds-number cavity flows, including some novel ones, and that can generate complex mixing patterns. The visualization of streamlines is standard and the results of mixing studies purely qualitative. In the first part we focus on steady flows and in the second on periodic flows. The objective of the second part is to suggest the possibility of developing chaotic mixing in two-dimensional flows.

2. Apparatus and experimental conditions

The geometries studied are shown in figure 1. A versatile apparatus, based on ideas originating from G. I. Taylor's (1934) 'four-roller' set-up, was designed to generate the flows. The system consists of two sets of roller pairs driven independently by reversible motors, and two neoprene bands. The flow region is adjustable up to a maximum area of 5×5.5 in by means of slots accompanying all the rollers and suitable partition blocks in the apparatus. The depth of the tank is approximately one foot. The motor drive (manufactured by B & B Motor and Control Corporation) has a $\frac{1}{8}$ HP motor supplied by a 115 V a.c. source. The connection of the motors to a SA-12 B & B motor control makes feasible reversible speeds of up to 173.0 r.p.m. If glycerine, which has a viscosity of 7.6 poise at 25 °C, is used as working fluid, Reynolds numbers between 0.1 to 100 can be produced (the neoprene bands limit the viscosity of the fluids that can be used). Replacing the partition blocks by rectangular acrylic sheets of various dimensions can result in converging or diverging flow or a combination of both. For our purposes the Reynolds number Re is defined as

$$Re = \frac{\rho V' H}{\eta} \frac{H}{W}, \tag{1}$$

where ρ is the density and η viscosity of the fluid and H is the height of a cavity. For non-rectangular cavities (such as figure 1*b*), H is the average of the two heights, i.e. $\frac{1}{2}(H_1 + H_2)$. W is the width of a cavity; V' is a characteristic velocity of the moving boundaries, which is equal to $\frac{1}{2}(|V_t| + |V_b|)$ if both walls are moving, where t and b refer to the top and bottom boundaries respectively.

The Reynolds number used in our experiments is the highest compatible with two competing effects: two-dimensionality of the flow and minimum diffusional spread of the dye in a given time. On one hand it is desirable to have Re as low as possible to avoid secondary flows and inertial effects, but in order to avoid the significant diffusion of the dye normal to the striations during the time of the experiment in a given cavity, the Reynolds number should be as large as possible. An order-of-magnitude calculation gives a Reynolds number of order one.

The photographic conditions for visualizing the flows of interest can be classified into two groups: (i) long-time exposure (approximately 90 s) of aluminum flakes to obtain streamlines of various flows,† and (ii) shot-by-shot recording of the deformation of a material line or a material blob. The former requires an extremely dark background, while the latter needs two sets of 600 W quartz lights shining from two sides of the tank. A Nikon FE2 coupled with a Nikkor microlens of 105 mm was used. A green filter enhanced the contrast between glycerine and red dye, which is made up of polymeric dye (by Warner–Jenkinson Corporation) and food colorant (by SCM Corporation) premixed with glycerine. The value of the diffusion coefficient of the dye in glycerine is estimated to be 10^{-8} cm^2/s. Figure 2 illustrates the design of the flow region.

The most important characteristic that we seek in this apparatus is the ability to produce two-dimensional flows. By using a transparent fluid, glycerine, and injecting tracer at different levels below the free surface, we were able to check for possible variations of the velocity with the depth. Although the use of a transparent fluid makes the photography considerably more difficult, it provides a good check on the

† See the comments given by Savaş (1985) on the difficulties of using reflective flakes for flow-visualization studies.

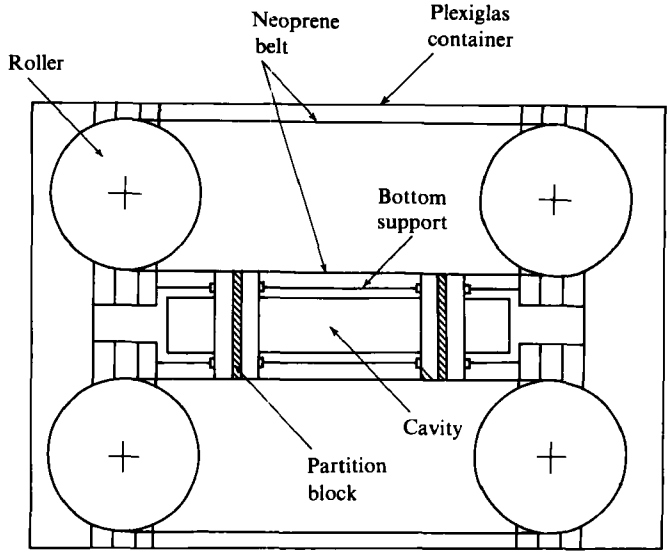

FIGURE 2. Diagram of the apparatus.

two-dimensionality of the flow. In most experiments a blob of a tracer was injected approximately 2–5 mm below the surface. Any deviation from two-dimensionality is cumulative, and in the case of alternating motion of the bands the separation of points is nearly exponential. Thus, deviations from two-dimensionality are easy to detect. In our case, and under most experimental conditions, they were found to be negligible, although it is possible to detect traces of this effect in some photographs.

Another point investigated was whether the elasticity of the bands was a significant effect during the experiments. Based on photographs of two sets of marks placed on the belt, the effect was found to be negligible.

3. Streamlines

Three types of streamlines were obtained; namely the standard cavity flow and two modifications. For the sake of convenience, the standard cavity flow is defined as Type I. A rectangular cavity with two sides moving in the same direction is referred to as Type II cavity flow, while a cavity with two sides moving in the opposite directions is called Type III (see figure 1). Figure 3(*a*) shows that the streamlines are closed and centred at approximately $(\frac{1}{2}W, \frac{2}{3}H)$. Figure 3(*b*) shows the streamlines of Type II cavity flow. For the case of $V_t = 1.86$ cm/s, and $V_b = 1.86$ cm/s, the vortices are near the upstreams of the moving boundaries. The streamlines of the Type III cavity flow are shown in Figure 3(*c*). Here, the inner loops of streamlines are circular, while the outer ones are almost rectangular. The Reynolds numbers, as defined above, are 0.6, 1.4 and 1.0 respectively for these three examples.

Streamlines of the above three configurations and corresponding Reynolds numbers were also obtained (see figure 4) by using a numerical scheme based on a finite-element method (Malone 1979). The agreement between the experimental results and the simulations is generally satisfactory.

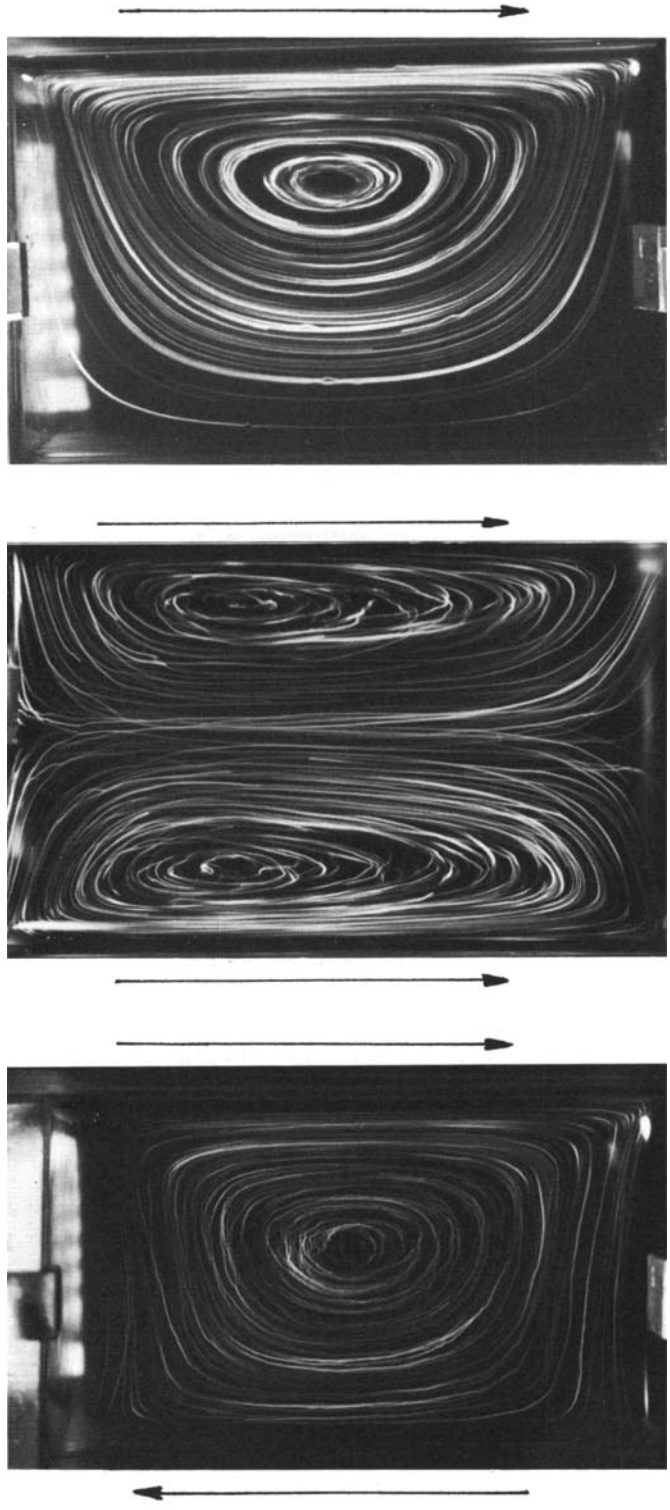

FIGURE 3. Streamlines of (*a*) Type I cavity flow, $W = 11.0$ cm, $H = 6.5$ cm, $V_t = 0.9$ cm/s, $Re = 0.6$; (*b*) Type II cavity flow, $W = 11.0$ cm, $H = 7.0$ cm, $V_t = 1.86$ cm/s, $V_b = 1.86$ cm/s, $Re = 1.4$; (*c*) Type III cavity flow, $W = 11.0$ cm, $H = 6.5$ cm, $V_t = 1.5$ cm/s, $V_b = -1.6$ cm/s, $Re = 1.0$.

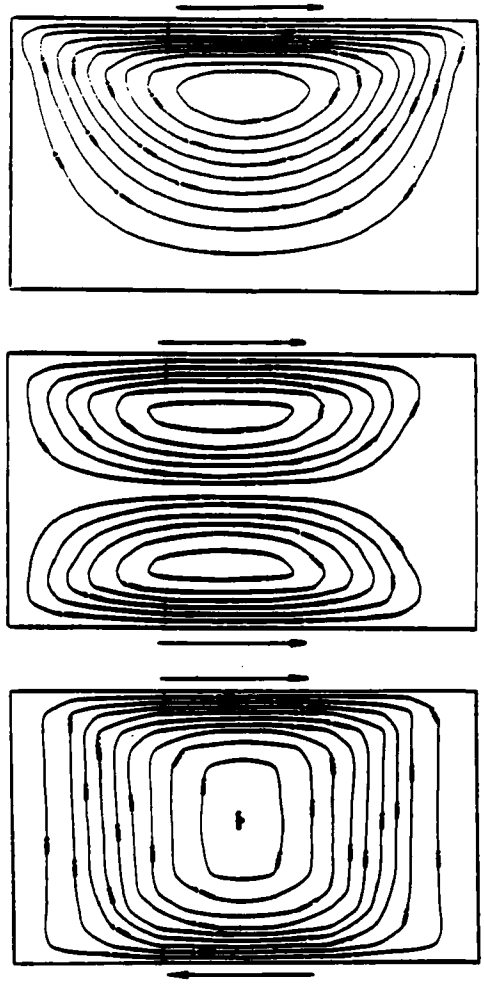

FIGURE 4. Computer simulation of streamlines in (*a*) Type I cavity flow; (*b*) Type II cavity flow; (*c*) Type III cavity flow with $|V_b/V_t| = 0.9$.

4. Chaotic Mixing

Recently, Aref (1984) indicated that the equations describing the motion of a fluid particle in a two-dimensional flow,

$$v_1 = \dot{x}_1 = \frac{\partial \Psi}{\partial x_2}, \quad v_2 = \dot{x}_2 = -\frac{\partial \Psi}{\partial x_1}, \tag{2}$$

Ψ, being the stream function, and ($\dot{}$) the material time derivative, are formally a Hamiltonian system with one degree of freedom if the system is autonomous, $\Psi(x_1, x_2)$, and with two degrees of freedom if the system is not autonomous, $\Psi(x_1, x_2, t)$. The solution of (2) with the initial condition $\boldsymbol{x} = \boldsymbol{X}$ ($\boldsymbol{x} = (x_1, x_2)$, $\boldsymbol{X} = (X_2, X_2)$) is $\boldsymbol{x} = \boldsymbol{F}_t \boldsymbol{X}$ and is called the *flow* in the theory of chaotic systems and the *motion* in continuum mechanics. Based on the theory of Hamiltonian systems the following statements can be made (see for example Guckenheimer & Holmes 1983):

If $\Psi = \Psi(x_1, x_2)$, the flow is *integrable* which implies zero Liapunov exponents and no chaos. However, if $\Psi = \Psi(x_1, x_2, t)$, the flow is likely to be *non-integrable*, which in turn implies the possibility of the flow being *chaotic*. If the flow is chaotic, the Liapunov exponents are positive and the stretching of material lines is exponential. (Note that non-integrability does not imply chaos, but non-integrability is a *necessary* condition for chaos). All integrable systems have poor efficiency, all chaotic systems have high efficiency (Chella & Ottino 1985*a*, *b*).

In the context of the theory of Hamiltonian systems, the word *chaotic* might be interpreted in any one of the following three ways: (i) positive Liapunov exponents in a given region of the flow; (ii) presence of transverse homoclinic or heteroclinic points; (iii) presence of Smale horseshoe functions. An accessible review of this is given by Doherty & Ottino (1986). For a deeper coverage, see Guckenheimer & Holmes (1983).

In our particular case, the easiest way to study chaos experimentally seems to be the detection of Smale horseshoe functions (Smale 1963, 1967). The Smale horseshoe functions involve the stretching and folding of a square onto itself. In the context of mixing in two-dimensional bounded flows the horseshoe function has a clear physical significance. However, the relationship with definitions (i) and (ii) as well as its mathematical implications are far from being obvious. For these matters the reader is referred to Moser (1973), and Guckenheimer & Holmes (1983).

Aref (1984) examined a model flow, the blinking vortex system, which according to numerical computations, leads to chaotic mixing. His system, as shown in figure 5(*a*), consists of two alternating corotating vortices each switched instantly on and off for a time $T_{\frac{1}{2}}$. The cavity flows with alternating motion of the boundaries can produce a somewhat analogous situation. (Obviously it takes some time for the motion to set in, $H^2/(\eta/\rho)$, of the order of 5×10^{-2} s. Nevertheless, in the experiments we wait for approximately 5 s between the motion of one band and the other to minimize the influence of transient effects.) As shown in figure 5(*b*), there is an elliptic fixed point at roughly $\frac{1}{3}H$ from the top. When the lower wall is moved, the point moves to a position $\frac{1}{3}H$ from the bottom. They resemble the two vortices of Aref's system. By analogy with the blinking vortex system, the experiments are quantified by means of the ratio of the dimensionless time of action of the boundary to the dimensionless time of redistribution in the cavity. This ratio is called the dimensionless frequency of oscillation f and is defined as

$$f = \frac{\dfrac{T_{\frac{1}{2}} V'}{W}}{\dfrac{27}{8}\dfrac{W}{H}} \tag{3}$$

where $(27/8)(W/H)$ is the dimensionless redistribution time in a cavity (Shearer 1973). The total time of the experiment is defined as T_{tot}; the total number of periods is $T_{\text{tot}}/2T_{\frac{1}{2}}$.

5. Experimental results for chaotic mixing

Two kinds of experiments are reported. The first is the deformation of material lines, the second the deformation of blobs (figures 6 and 7). Material lines provide information about mixing, and for the steady-state flows they can be readily compared with the streamlines of figures 3(*a–c*). In steady flows the material is trapped between streamlines and the material line slowly orients in a direction

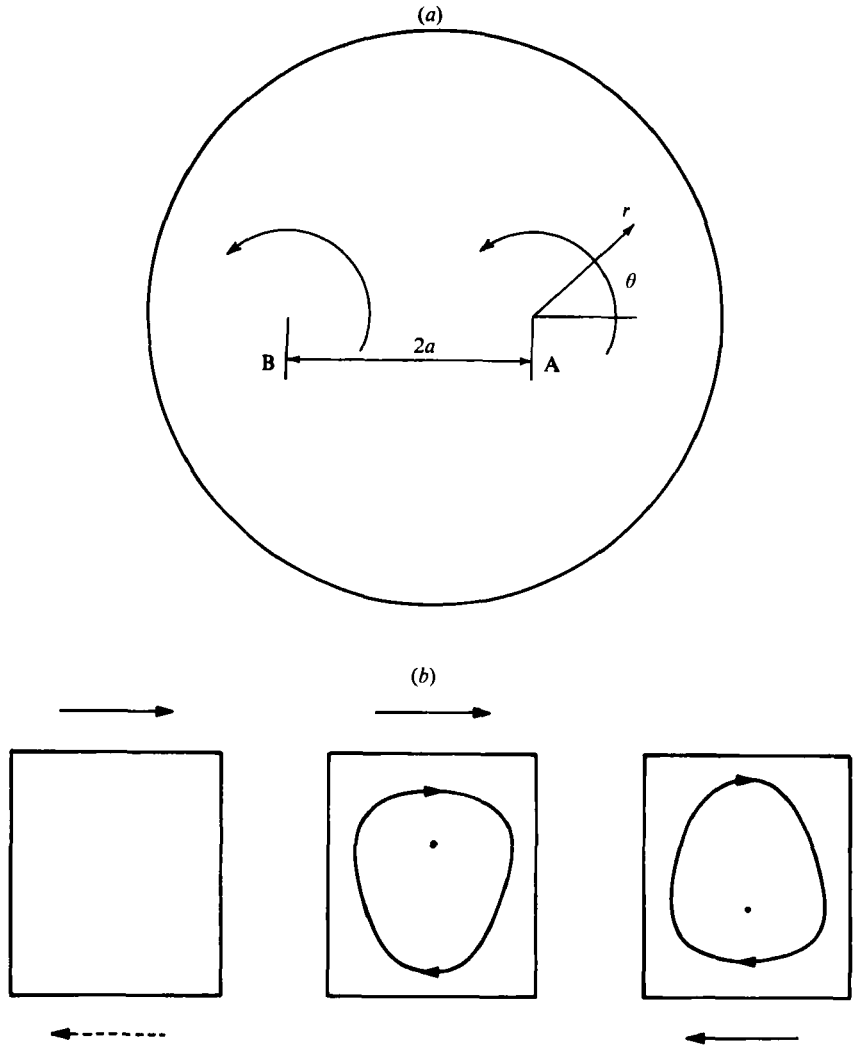

FIGURE 5. Comparison of (a) Aref's (1984) blinking vortex and (b) the alternate periodic cavity.

tangential to them. This implies decay of mixing efficiency and the stretching is very ineffective (Chella & Ottino 1985*a*). As shown in figure 6(*d*), the alternate periodic cavity flow, however, can result in much more effective and uniform dispersion of the material line.

The deformation of blobs is central to the understanding of mixing and provides information about horseshoe functions. Results are very sensitive to the period of the motion. For the cases of $T_{\frac{1}{2}} = 10$, 20, and 30, s corresponding to dimensionless frequencies of recirculation of 0.3, 0.6 and 0.9 respectively, it is found that the efficiency of mixing strongly depends on the value of f (see figure 7). As the half-period is further increased, surpassing the total time of the experiment (e.g. 300 s in figure 7), the flow becomes a standard cavity flow, which is a very inefficient way of mixing. It is therefore concluded that there exists an optimal value of f to achieve the best mixing in a given time. For this particular cavity the optimum seems to lie between

0.6 and 0.9. Figure 6(*d*) with $f = 0.66$ produced excellent mixing. Figure 8(*a*), also with $f = 0.66$, again produced excellent mixing.

The effect of boundary geometry was also studied. Keeping the value of f constant (for example $f = 0.66$ in figure 8), a small variation of boundary geometry – trapezoidal cavity, figure 1(*b*) – can produce a substantial change in the final result of mixing. Lower or higher values of f seem to magnify this effect.

The initial location of the material blob is also important and is analysed in figures 9(*a–c*). It appears that the initial location of a material blob is crucial to the final state of mixing when f is not close to the optimum. Examples are given in figures 8(*b*) and 9(*a*) ($f = 0.66$). Both cases are compared at the same times, which are 0, 1, 2 and 5 min respectively, and the final results at 5 min do not vary very much. For a somewhat lower value of f the effect of initial location on the deformation of the material blob seems to be more important (see figures 9*b*, *c*). An even lower value would magnify this effect.

The investigation of horseshoe functions is given in figure 10 (for the mathematical aspects of horseshoe functions and their applications in mixing see Rising & Ottino 1986). The existence of horseshoes in a given region of the flow can be checked and, in theory, proven by superimposing photographs of forward and backward transformations with the initial location of the blob. If the resultant construction produces a horseshoe function, i.e. if it satisfies Moser's conditions (Moser 1973), then, according to our previous definition, the cavity flow displays chaotic behaviour in that region. Note that we are assuming that we have a periodic flow and are referring to the map from the initial conditions to the locations at $t = 2T_{\frac{1}{2}}$ (complete period) and $t = -2T_{\frac{1}{2}}$ as the forward and backward transformations respectively. This mapping is known as a 'time one return map' or *Poincaré section* of the flow (cf. e.g. Guckenheimer & Holmes 1983). From a practical viewpoint this implies that since the flow is periodic and forms a horseshoe, a very fine subdivision of the blob will occur in the region initially occupied by the blob. Obviously it is desirable that the flow forms several horseshoe functions, possibly interacting, in such a way that they influence a large portion of the mixing region. From the point of view of mixing it is also desirable that they be of low period (the period being the number of transformations needed to produce the horseshoe) since we want to achieve good mixing as quickly as possible, and since the domain of influence of a high-period horseshoe is usually small.

There are several properties that must be verified to deduce the presence of a horseshoe function in a mixing system (Moser's conditions, Moser 1973):

(i) A quadrilateral S and a period p must be found such that the intersection of the quadrilateral, its forward image, $F^p(S)$, and its inverse image, $F^{-p}(S)$, produce a picture such as figure 11(*a*). The number of striations in each image is greater than or equal to two. The method for doing this is to choose a region of the flow likely to contain a horseshoe by finding a quadrilateral in the intersecting streamlines (for alternating flows, see figure 11*b*), with hyperbolic points at opposing vertices (this structure is present during the onset behaviour for horseshoes in these flows).

(ii) It must be verified that the forward striations are the images of the inverse striations, and that the top and bottom of each forward striation is an image of the top or bottom of an inverse striation after the flow moves for a period of the horseshoe. This usually involves careful examination of photographs taken at each full and half period. If video recording is available or if the flow is directly observed the experimenter may be able to verify this move easily, and choose the appropriate pictures to demonstrate that the condition is fulfilled.

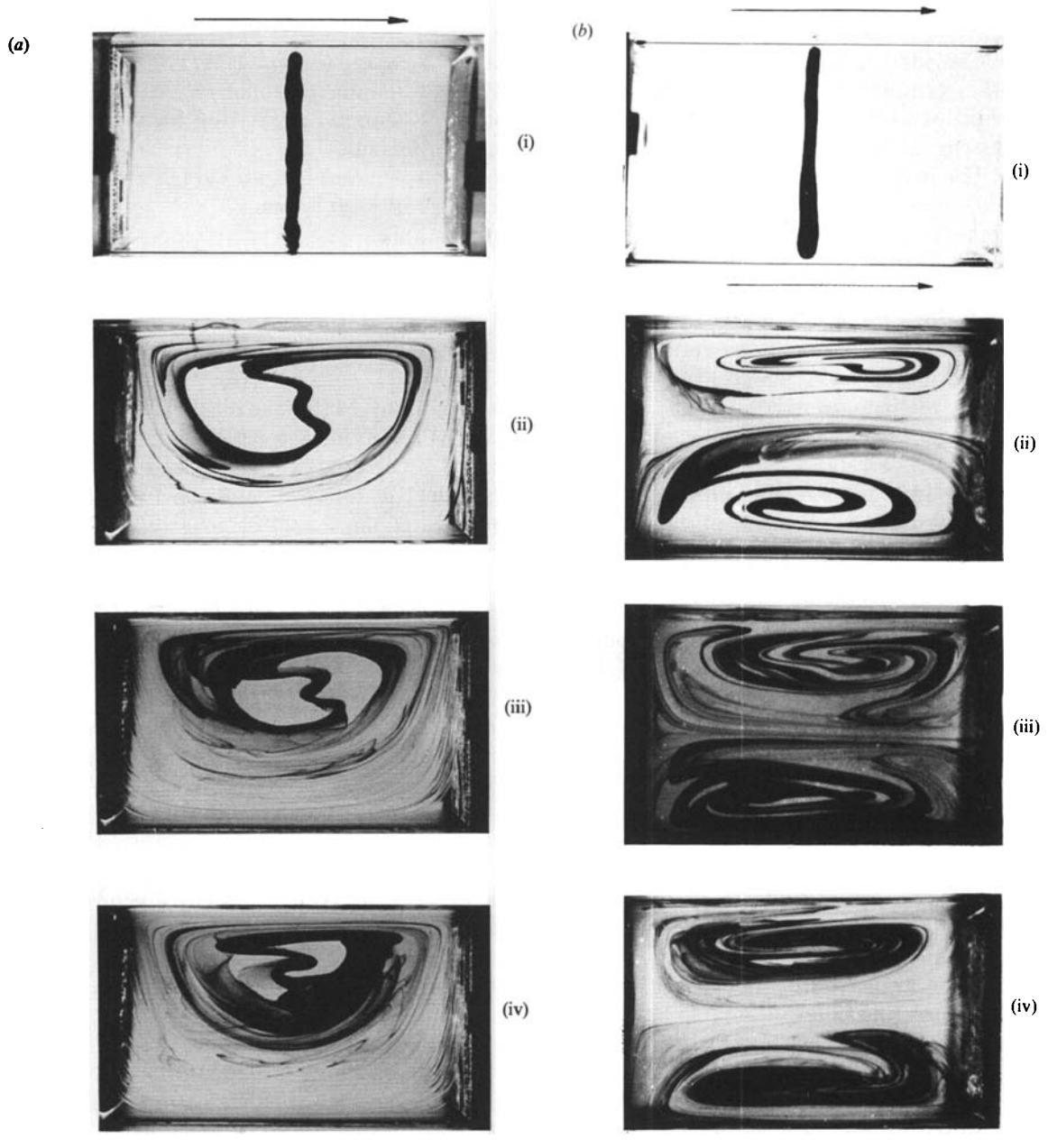

FIGURE 6 (*a*, *b*). For caption see facing page.

(iii) After running the flow through another period forward, the image of each forward striation must have a striation properly contained in each forward striation, and running the flow backward must produce the same effect with respect to the inverse striations. Each of these must be of width strictly less than the striation containing it.

(iv) In a coordinate frame consistent with the boundaries of the quadrilateral (e.g. for the construction mentioned in (i) the coordinates are the intersecting streamlines,

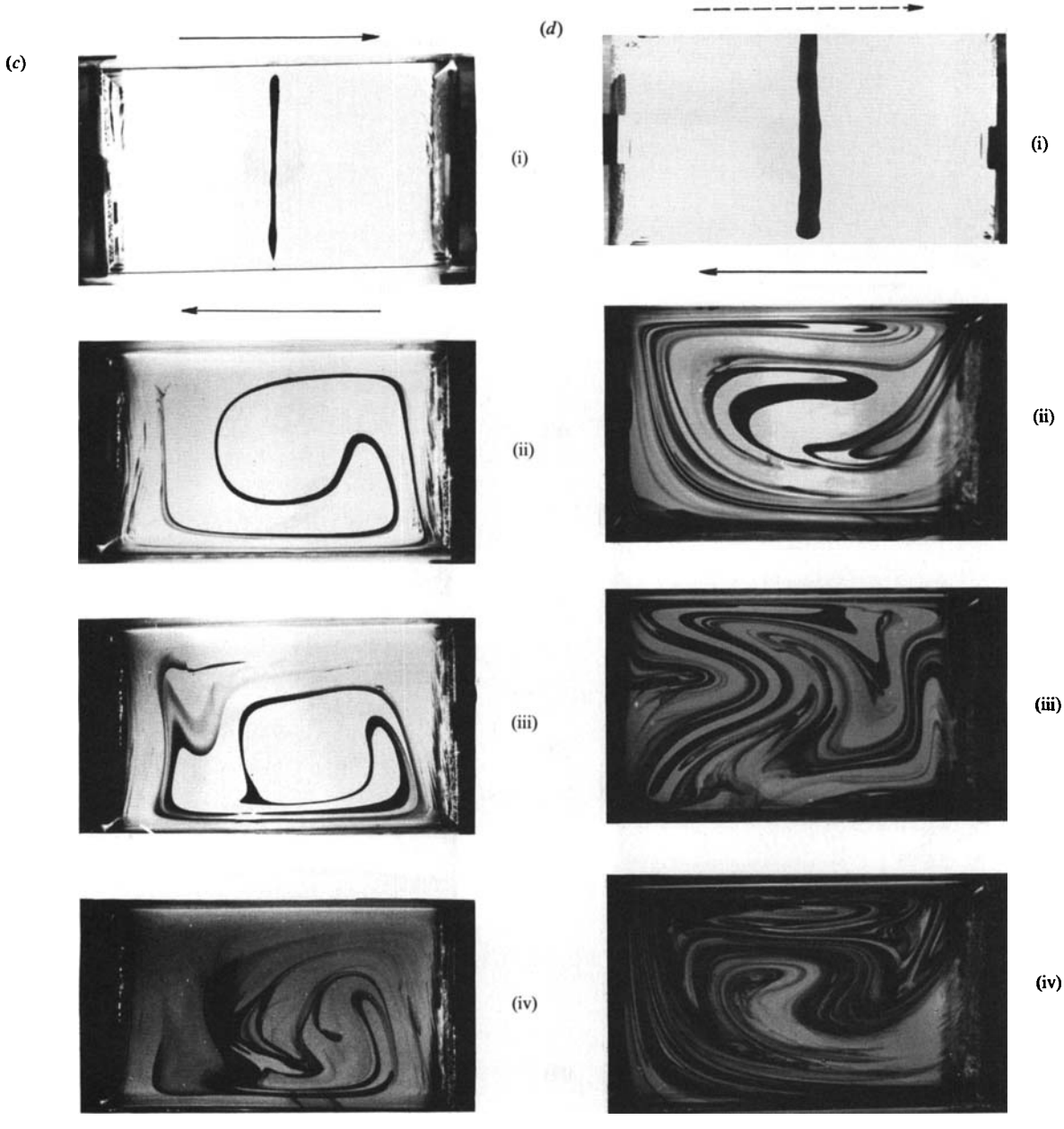

FIGURE 6. Deformation of a material line in (*a*) Type I cavity flow, $W = 10.5$ cm, $H = 6.5$ cm, $V_t = 1.65$ cm/s, $Re = 1.1$; (*b*) Type II cavity flow, $W = 10.5$ cm, $H = 6.5$ cm, $V_t = 1.65$ cm/s, $V_b = 2.0$ cm/s, $Re = 1.2$; (*c*) Type III cavity flow, $W = 10.5$ cm, $H = 6.5$ cm, $V_t = 1.65$ cm/s, $V_b = -2.0$ cm/s, $Re = 1.2$; and (*d*) alternate periodic cavity flow, $W = 10.5$ cm, $H = 6.5$ cm, $V_t = 1.65$ cm/s, $V_b = -2.0$ cm/s, $f = 0.66$; at (i) initial state, (ii) 60 s, (iii) 120 s, and (iv) 300 s. $T_{tot}/2T_{\frac{1}{2}} = 7.5$.

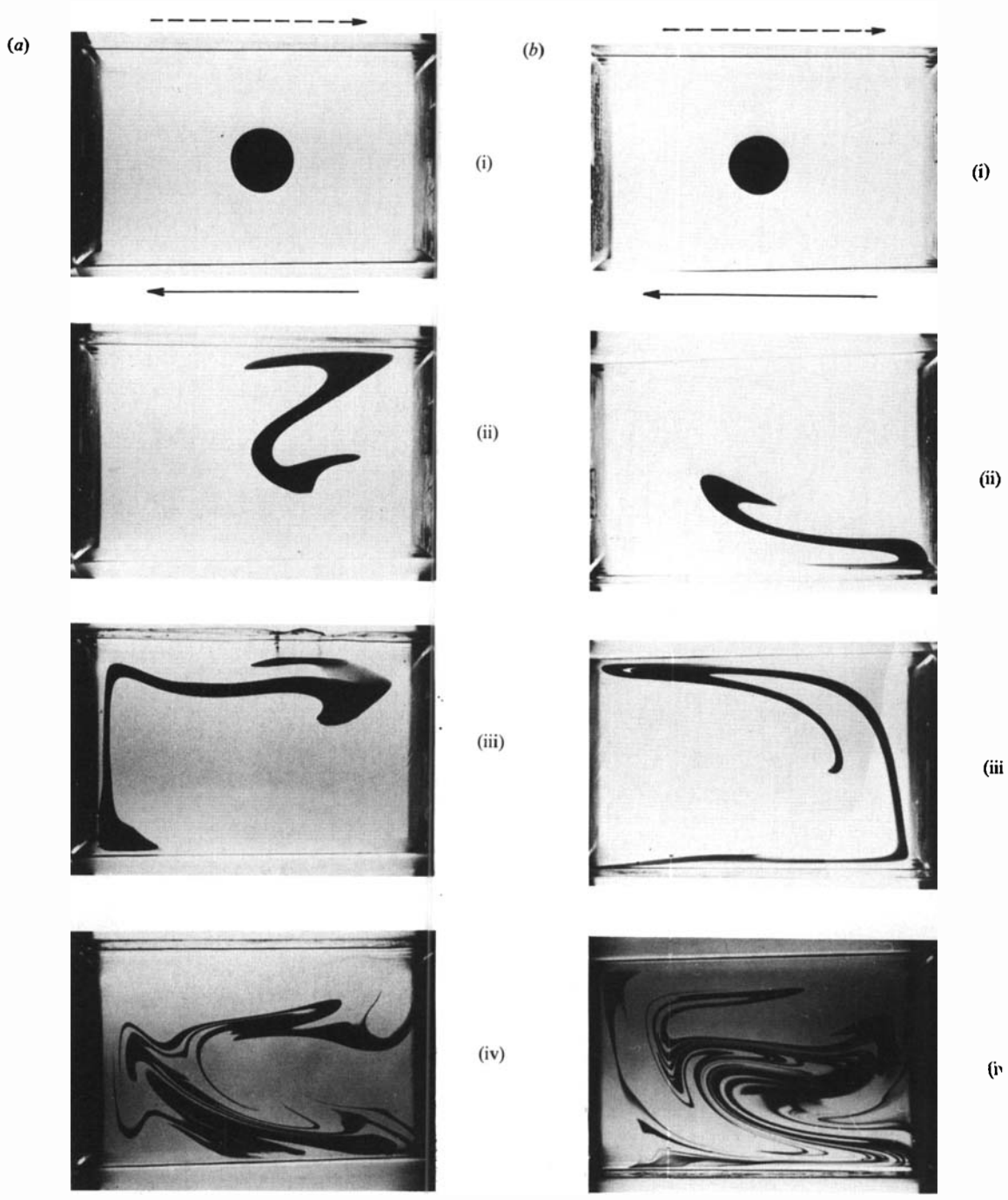

FIGURE 7 (a, b). For caption see facing page.

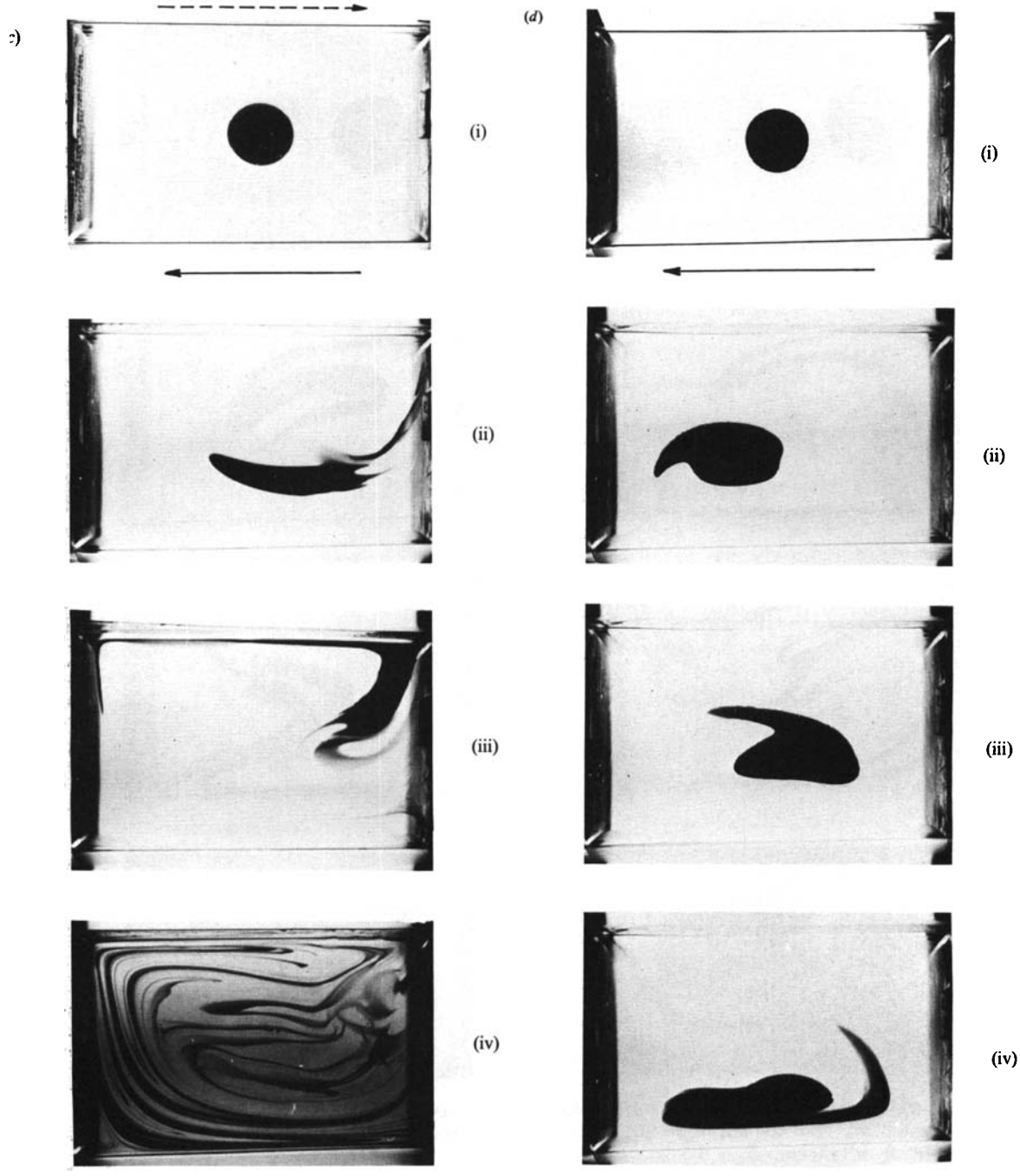

FIGURE 7. Deformation of a material blob for various f values. $W = 10.5$ cm, $H = 7.0$ cm, $V_t = 1.59$ cm/s, $V_b = -1.59$ cm/s, $Re = 1.23$. (*a*) $T_{\frac{1}{2}} = 10$ s, $f = 0.3$, $T_{tot}/2T_{\frac{1}{2}} = 15$; (*b*) $T_{\frac{1}{2}} = 20$ s, $f = 0.6$, $T_{tot}/2T_{\frac{1}{2}} = 7.5$; (*c*) $T_{\frac{1}{2}} = 30$ s, $f = 0.9$, $T_{tot}/2T_{\frac{1}{2}} = 5$; and (*d*) $T_{\frac{1}{2}} > T_{tot}$; at (i) initial state, (ii) 60 s, (iii) 120 s, and (iv) 300 s.

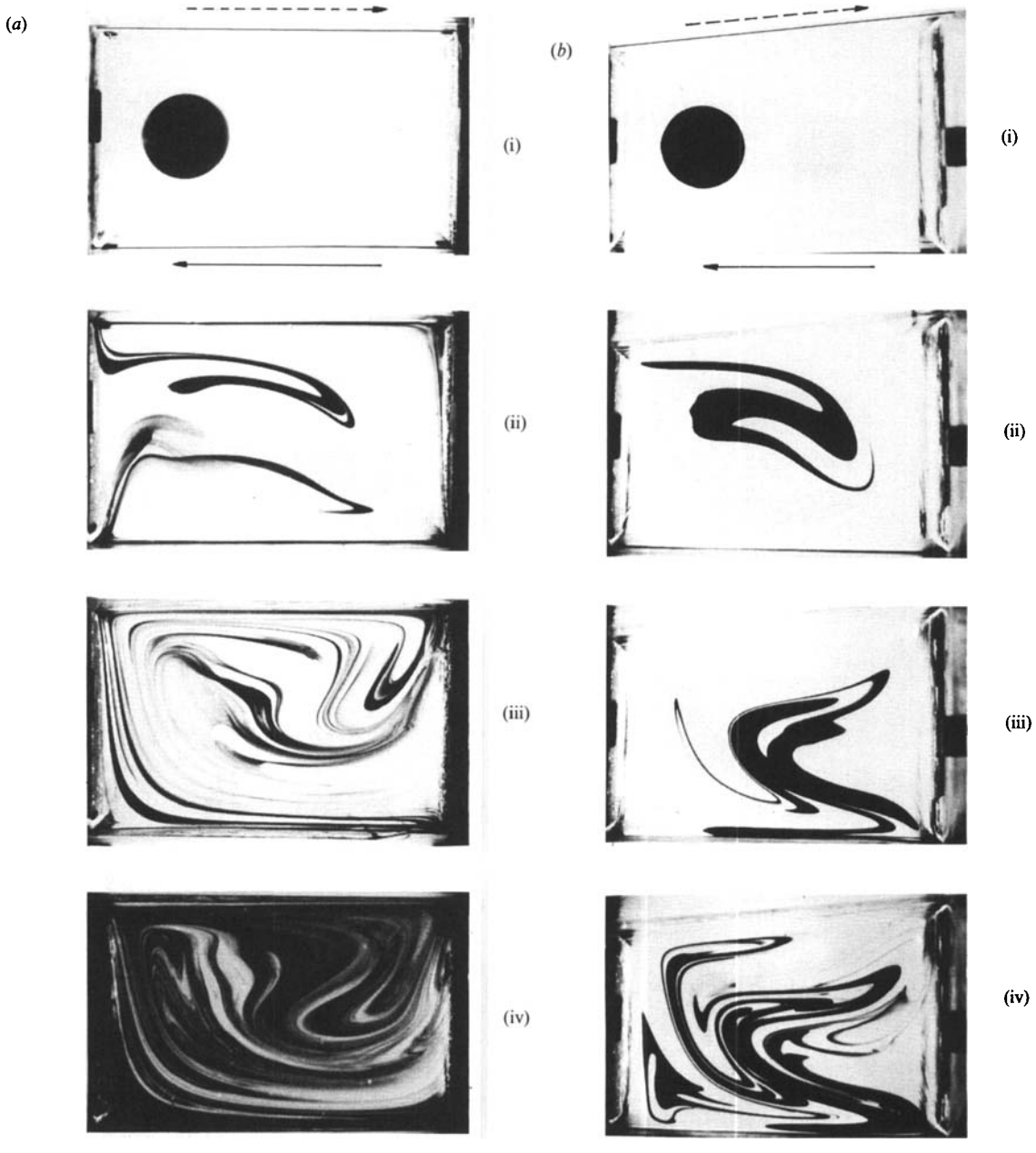

FIGURE 8. Deformation of a material blob for various geometries at the same f value. (a) $W = 10.5$ cm, $H = 6.5$ cm, $V_t = 1.90$ cm/s, $V_b = -1.90$ cm/s, $T_{\frac{1}{2}} = 20$ s, $f = 0.66$; (b) one-side tilted, $W = 11.0$ cm, $H_1 = 6.5$ cm, $H_2 = 7.8$ cm, $V_t = 1.90$ cm/s, $V_b = -1.90$ cm/s, $T_{\frac{1}{2}} = 20$ s, $f = 0.66$; at (i) initial state, (ii) 60 s, (iii) 120 s, (iv) 320 s. $T_{tot}/2T_{\frac{1}{2}} = 8$.

figure 11 b) the boundaries of the forward and inverse striations must cross at an angle θ of roughly 19° or more to ensure that all future striations will intersect at sufficient angle and to guarantee that all periodic points are hyperbolic. (The condition here is that the slope of vertical boundaries be greater than $1/\mu$ and the horizontal boundaries have slope less than μ. For area preserving system μ satisfies $1 < 2/\mu^2$, Moser 1973).

As with Aref's system (Aref 1984), these conditions are met for lower and lower period as the flow strength in the cavity flow, which corresponds to the dimensionless frequency of oscillation f, is increased from zero. The system is more complicated than Aref's system in that the speed along streamlines for each half period is not constant. It can be shown that when structures analogous to those in the Aref's model are present in a region where the speed along streamlines is less than the mean speed of each, the conditions for horseshoe functions are met more stringently (Rising & Ottino 1986). For the particular cavity flow in figure 10(*c*) we are thus expecting the horseshoe in the location shown for some value of f and the experimental method is a verification of this. For systems in which such prior knowledge is unavailable, sufficiently refined experimental technique, tailored to the particular system in question, should be capable of proving the existence of the horseshoe by itself. We analyse below the photographs given here with this in mind as they suggest both methods and difficulties.

Experimentally, the most difficult conditions to verify are that the forward top is the image of the inverse top or bottom (i.e. condition (ii)), and that the subsequent forward images lie inside (i.e. the first part of condition (iii)). In systems other than alternating flows, construction of the quadrilateral and determination of period are also subject to the same difficulties and may require a fair amount of intuition or experiment to unravel. The major problem lies in placing the blobs directly on the horseshoe structure. If they do not coincide, the result is that individual striations may be either dye-filled, partially filled or empty.

To verify condition (ii) the technique used was to conjecture the correspondence of pieces of the blob between many photographs and verify the conjecture by watching the experiment in motion. When the blob placement is not exact, two effects should be considered. The first is that the horseshoe structure takes several periods to be visible. This is because the dye must be drawn into the horseshoe before it begins to striate. The period at which the striations begin is then higher than the period of the horseshoe. If the horseshoe has n striations, it should have n^k after k periods. The blob is incorrectly placed if it is inconsistent with m^k, where m is the first period at which it striates. The second effect is that each striation is only partially filled so that the striations of dye will tend to violate condition (iii) by moving inward or outward on each transformation instead of overlapping properly. *Consistent* movement towards the centre or outside the horseshoe is the result. This can be overcome by keeping track of both filled and empty striations and combining them to foresee a reasonable picture. Comparison of the initial position of the dye with that of a conjectured horseshoe should confirm that this has been done properly. These problems are both present in figure 10 where the blob intersects the corner of the horseshoe instead of lying directly on top of it. Final verification of the horseshoe set is possible experimentally if the dye is placed as carefully as possible in the quadrilateral so that alternately all the striations will be filled, as shown in figure 12. For the cavity flow the period 1 horseshoe appears to form between $f = 0.4$ and 0.6. It changes from horseshoe type $(1, -2)$ to type $(1, 2)$ to type $(1, 2, -3)$, shown in figure 13, between $f = 0.6$ and 0.8 (this notation is developed by Rising & Ottino 1986.) This is consistent with systems like the Aref's in which varying the flow strength causes innumerable horseshoes to form, collapse and coalesce into other horseshoe structures. Visual observation is very enlighting and provides the experimentalists with considerable insight into formation and change of the horseshoe functions present. Varying the geometry and period to give the best complete horseshoe function may or may not improve the mixing. The reasons for this are that improving the angle and stretch to improve the horseshoe may in some cases so

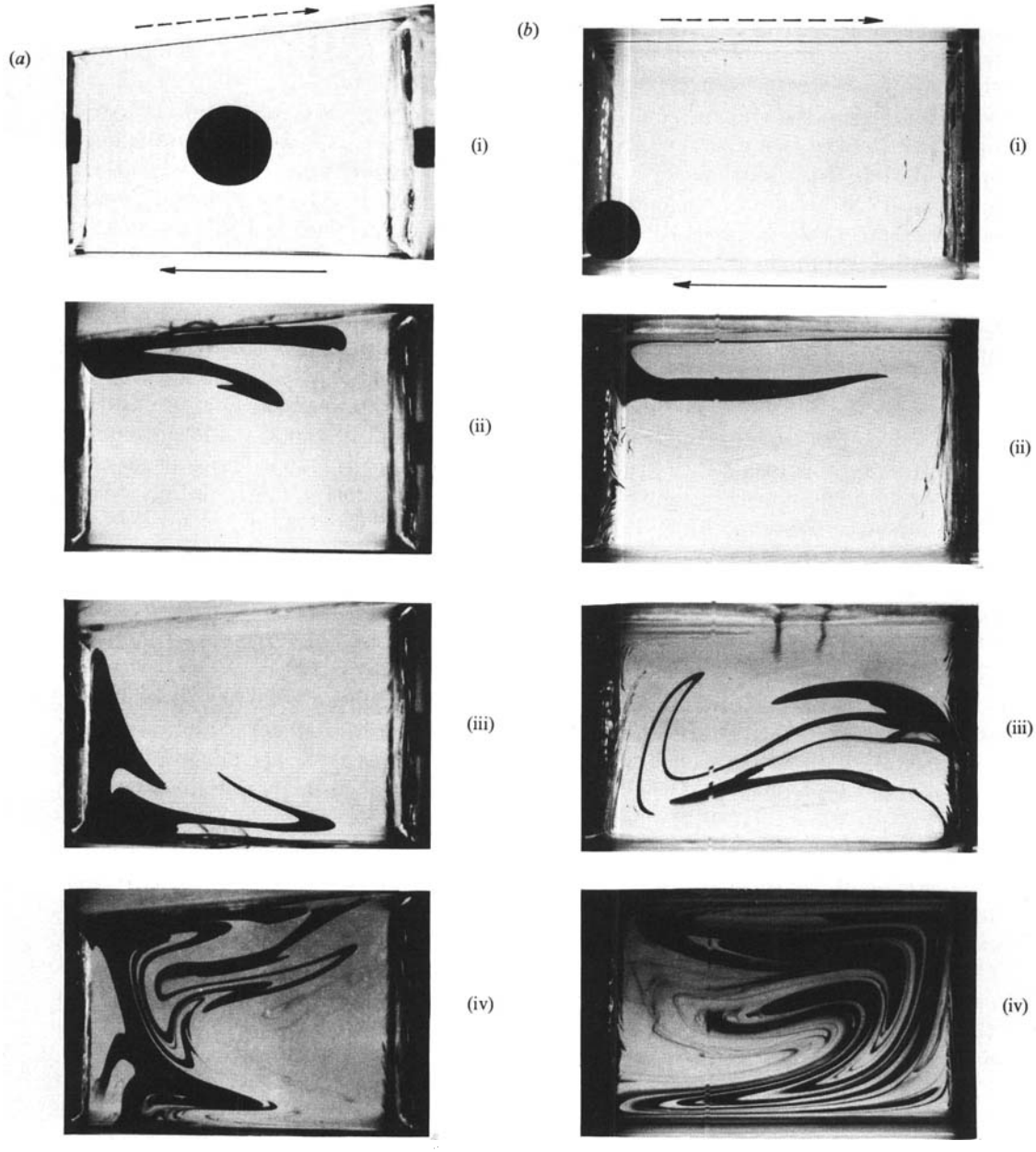

FIGURE 9 (*a*, *b*). For caption see facing page.

drastically reduce the striation width that the mixing influences only a small part of the fluid. Also, although the (1, 2) horseshoe is qualitatively a better mixing device than the (1, −2) horseshoe, its development may coincide with loss of good mixing in other parts of the cavity.

The computation of the backward transformations from the forward transformations brings us to an important point which appears in both experimental and computational aspects of the problem: can a picture such as figure 10(*b*) be unscrambled and restored to its initial configuration, figure 10(*a*)? Obviously in the

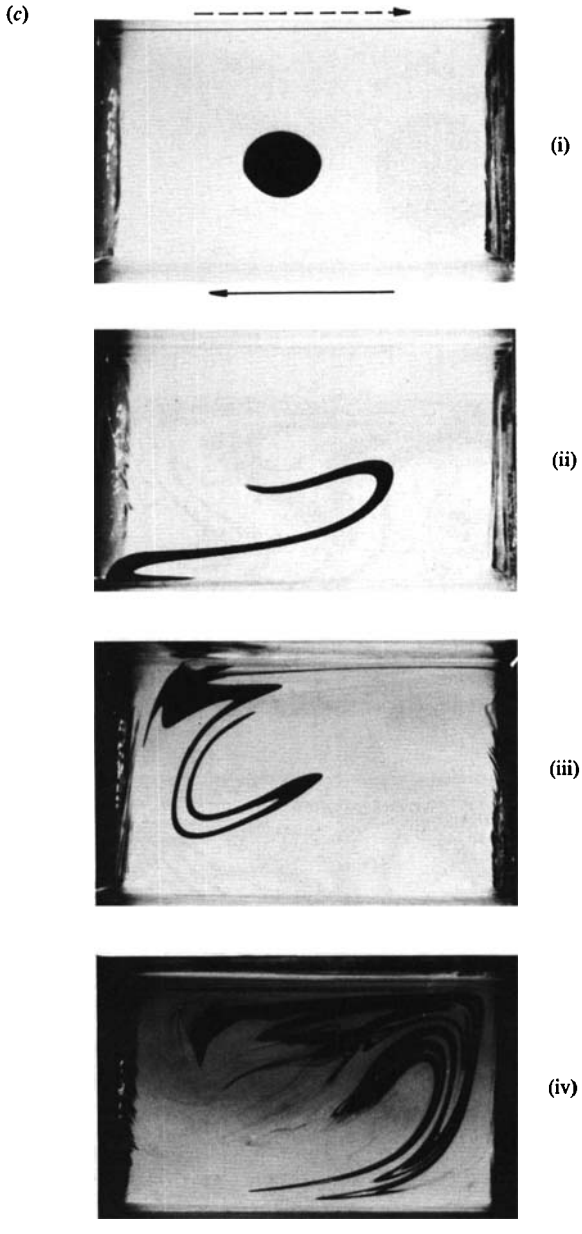

FIGURE 9. Deformation of a material blob placed at different initial locations. (*a*) $W = 11.0$ cm, $H_1 = 6.5$ cm, $H_2 = 7.8$ cm, $V_t = 1.90$ cm/s, $V_b = -1.90$ cm/s, $T_{\frac{1}{2}} = 20$ s, $f = 0.66$; (*b*) $W = 11.0$ cm, $H = 7.0$ cm, $V_t = 1.3$ cm/s, $V_b = -0.9$ cm/s, $T_{\frac{1}{2}} = 20$ s, $f = 0.4$; (*c*) $W = 11.0$ cm, $H = 7.0$ cm, $V_t = 1.3$ cm/s, $V_b = -0.9$ cm/s, $T_{\frac{1}{2}} = 20$ s, $f = 0.4$; at (i) initial state, (ii) 60 s, (iii) 120 s, and (iv) 300 s. $T_{tot}/2T_{\frac{1}{2}} = 7.5$.

experimental case there is molecular diffusion which is of course irreversible. But neglecting this aspect, since the problem is deterministic, in principle it can be done. However, if the system is chaotic, e.g. contains horseshoe sets, the problem becomes sensitive to initial conditions (nearby trajectories diverge exponentially). Computations are reversible only with infinite precision. With finite precision, a finite time

FIGURE 10. Detection of horseshoe functions. $W = 10.5$ cm, $H = 6.5$ cm, $V_t = 1.9$ cm/s, $V_b = -1.9$ cm/s, $T_{\frac{1}{2}} = 20$ s, $f = 0.66$; at (*a*) initial state, (*b*) 160 s, (*c*) overlap of the forward and backward transformations, (*d*) enlargement of horseshoe function in (*c*).

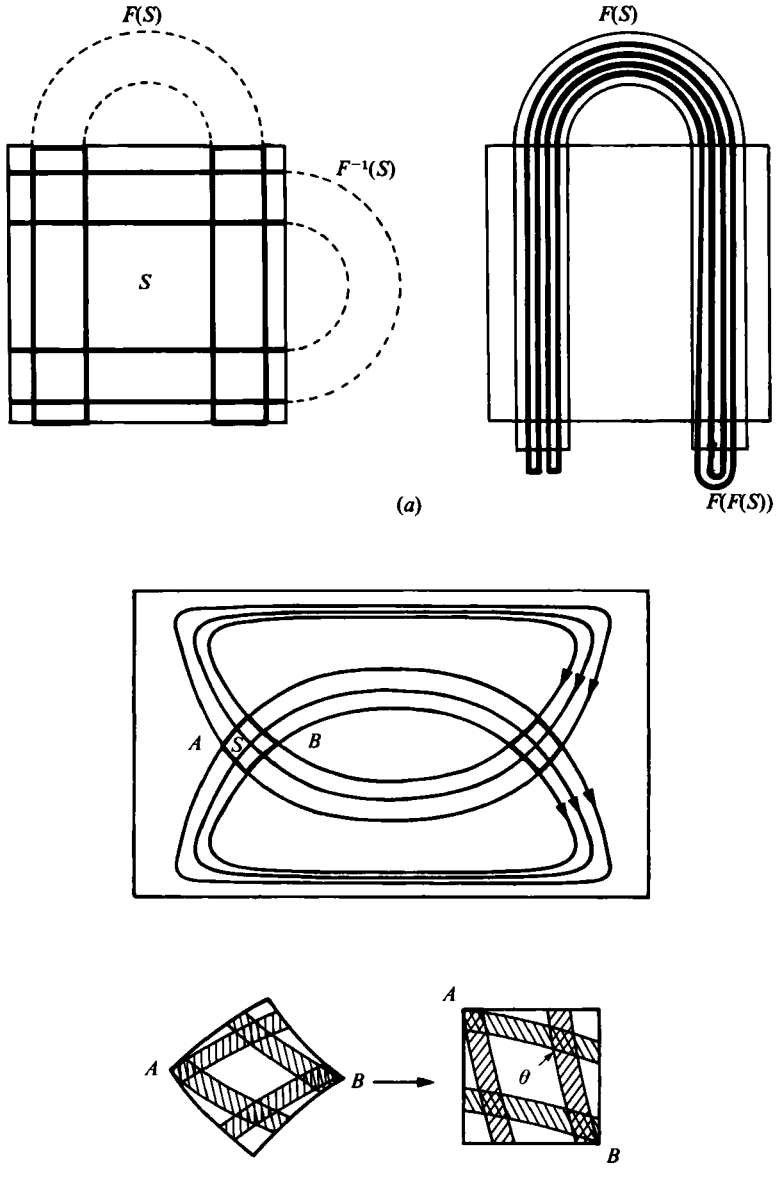

FIGURE 11. (*a*) Properties (ii) and (iii) (see text). The images of tops and bottoms of the inverse striations must be tops and bottoms of forward striations. The successive forward striations must lie inside those of the previous transformation with a uniform decrease in area. $F(S)$ is the forward transformation, $F^{-1}(S)$ the backward transformation. (*b*) Quadrilateral S formed by the streamlines in alternate periodic cavity flow. A and B are hyperbolic points.

T can always be found beyond which the initial condition is lost, and the problem cannot be restored. For numerical calculations, with N-bit precision, the initial condition is lost after $O(2^N)$ transformations in regular systems and $O(N)$ in chaotic systems. Loosely speaking, an integrable or regular system is computationally reversible but a chaotic one is not. A computational example in the context of mixing is given by Khakhar, Chella & Ottino (1984). The same point was raised by Aref

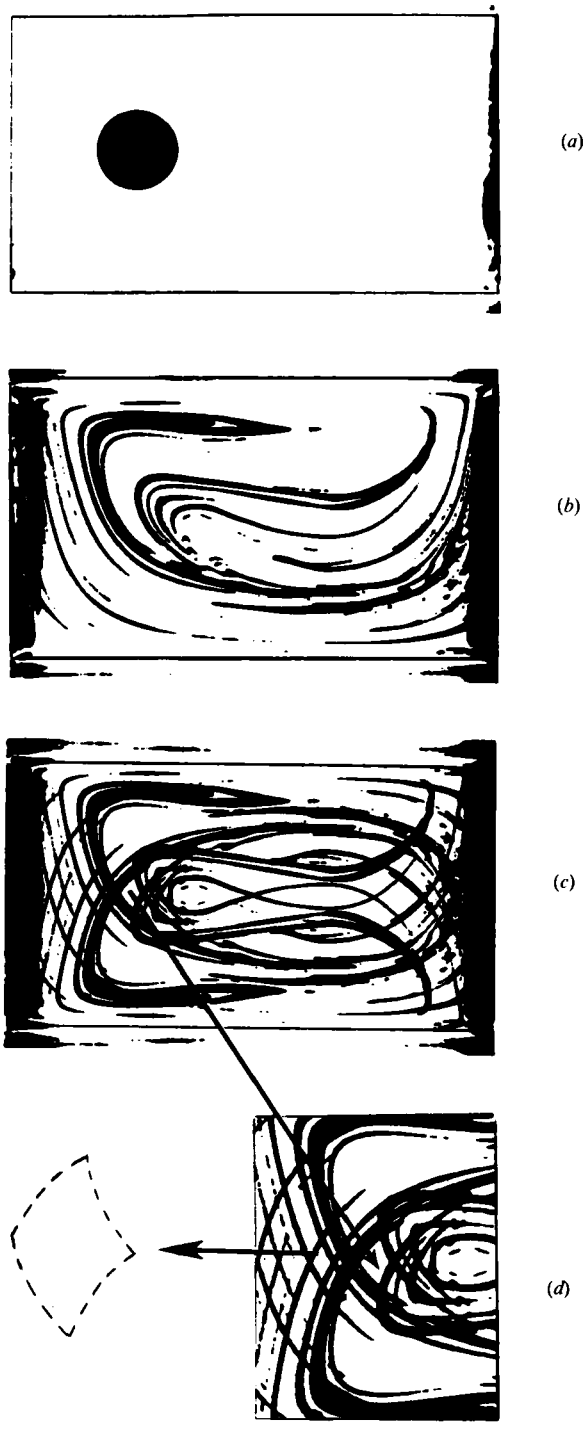

FIGURE 12. Same as figure 10 but changing the location of the blob.

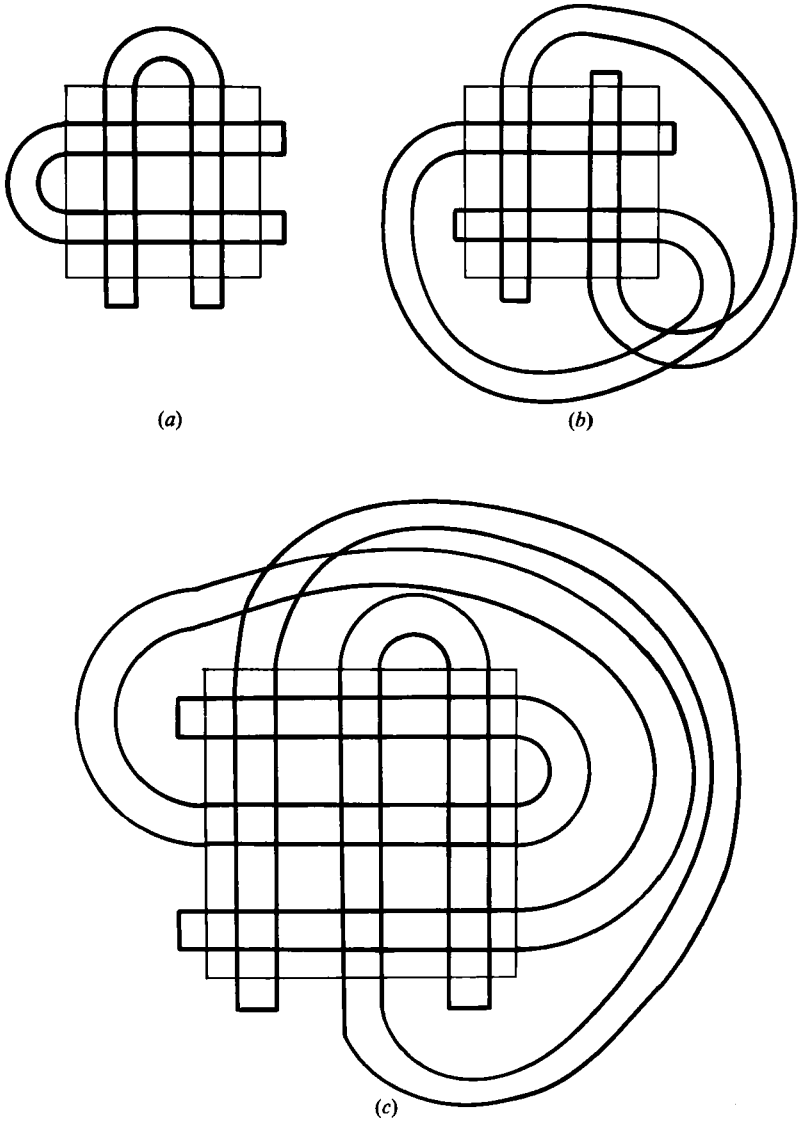

FIGURE 13. (*a*) Schematic of S, $F(S)$, and $F^{-1}(S)$ for a $(1, -2)$ horseshoe. (*b*) Schematic of S, $F(S)$, and $F^{-1}(S)$ for a (1,2) horseshoe. (*c*) Schematic of S, $F(S)$, and $F^{-1}(S)$ for a $(1, 2, -3)$ horseshoe. $F(S)$ is the forward transformation, $F^{-1}(S)$ the backward transformation.

(1984). Experimentally one can unscramble – within experimental error – figures 6*a*(iv), 6*b*(iv) and 6*c*(iv), but it is much harder to reverse 6*d*(iv). Thus the issue of kinematical reversibility of creeping flows should be treated with caution.

6. Conclusions

The alternate (periodic) cavity flow was found to be much more efficient than steady flows (Types I, II and III, figure 1). This is not surprising since *all* steady two-dimensional flows are integrable and hence have zero Liapunov exponents and consequently time-decaying efficiencies. On the other hand, the alternate (periodic)

cavity flow can produce horseshoe functions and hence chaos. However, we are unable to predict the region of global chaos and can not generate good overall mixing.

For low Reynolds numbers, the dimensionless frequency of oscillation f seems to be the most important parameter to compare among various flows. It seems clear that there exists an optimal value of f that is able to produce the maximum stretching in a given time (if $f \to 0$ the flow becomes integrable and the size of the chaotic region should go to zero; if $T_{\frac{1}{2}} > T_{\text{tot}}$ the flow is again integrable). In some model flows it is possible to compute this value. For long mixing times there seems to be an optimal value of f that produces the maximum stretching with the minimum expenditure of energy (Khakhar, Rising & Ottino 1985). For flows such as the cavity flow, we are not able to predict the optimal value of f.

All other things being equal, the geometry of the flow region seems to be an important factor in deciding the final results of mixing; mixing of blobs provides most information. For example, we found that the alternate (periodic) cavity flow becomes less efficient when one of the boundaries is tilted. This effect is noticeable even for 'optimal' values of f. The initial location does not seem to be critical when the system operates at an optimal value of f.

There are currently many difficulties with a theoretical treatment of optimizing the mixing conditions caused by horseshoes. However, the possibility of locating them experimentally provides new information on mixing properties, and thus new input for theoretical treatment. Since horseshoe functions can be located experimentally, this method allows the qualitative treatment of mixing of more complex flows than can usually be understood analytically through the equations of motion.

The authors take pleasure in acknowledging the financial support of the National Science Foundation in the form of a PYI award (CPE-8351096) and the Department of Energy (DE-FG02-85ER13333). Dr M. F. Malone's suggestions on the numerical simulations and comments on an earlier version of the manuscript are greatly appreciated.

REFERENCES

AREF, H. 1984 Stirring by chaotic advection. *J. Fluid Mech* **143**, 1–21.

BIGG, D. & MIDDLEMAN, S. 1974 Laminar mixing of a pair of fluids in a rectangular cavity. *Ind. Engng. Chem. Fundam.* **13**, 184–190.

BURGGRAF, O. C. 1966 Analytical and numerical studies of the structure of steady separated flows. *J. Fluid Mech.* **24**, 113–151.

CHELLA, R. & OTTINO, J. M. 1985*a* Fluid mechanics of mixing in a single screw extruder. *Ind. Engng. Chem. Fundam.* **24**, 170–180.

CHELLA, R. & OTTINO, J. M. 1985*b* Stretching in some classes of fluid motions and asymptotic mixing efficiencies as a measure of flow classification. *Arch. Rat Mech. Anal.* **90**, 15–42.

DOHERTY, M. F. & OTTINO, J. M. 1986 Chaos in deterministic systems: strange attractors, turbulence, and applications in chemical engineering. *Chem. Engng. Sci.* (to appear).

GREENSPAN, D. 1974 *Discrete Numerical Methods in Physics and Engineering.* Academic.

GUCKENHEIMER, J. & HOLMES, P. 1983 *Nonlinear Oscillations, Dynamical Systems, and Bifurcations of Vector Fields.* Springer.

HARLOW, F. H. & AMSDEN, A. A. 1970 The MAC methods. *Los Alamos Scientific Laboratory Monograph* LA-4370.

KHAKHAR, D. V., RISING, H. & OTTINO, J. M. 1986 An analysis of chaotic mixing in two model flows. *J. Fluid Mech.* (in press).

KHAKHAR, D. V., CHELLA, R. & OTTINO, J. M. 1984 Stretching, chaotic motion and breakup of elongated droplets in time dependent flows. *Adv. Rheology*, vol. 2, (Fluids), pp. 81–88, *Proc. IX Intl. Congress of Rheology* (ed. B. Mena, A. Garcia-Rejon & C. Rangel-Nafaile). Universidad Autonoma de Mexico.

MALONE, M. F. 1979 Numerical simulation of hydrodynamics problems in polymer processing. Ph.D. thesis, University of Massachusetts, Amherst, MA.

MIDDLEMAN, S. 1977 *Fundamentals of Polymer Processing*. McGraw-Hill.

MOSER, J. 1973 *Stable and Random Motions in Dynamical Systems*. Princeton University Press.

NALLASAMY, M. & PRASAD, K. K. 1977 On cavity flow at high Reynolds numbers. *J. Fluid Mech.* **79**, 391–414.

OTTINO, J. M. & CHELLA, R. 1983 Laminar mixing of polymeric liquids: brief review and recent theoretical developments. *Polym. Engng. Sci.* **23**, 357–379.

PAN, F. & ACRIVOS, A. 1967 Steady flows in rectangular cavities. *J. Fluid Mech*, **28**, 643–655.

PEYRET, R. & TAYLOR, T. D. 1983 *Computational Methods of Fluid Flow*. Springer.

RISING, H. & OTTINO, J. M. 1986 The use of horseshoe functions in mixing studies. *Physica* D (in preparation).

SAVAŞ, Ö. 1985 On flow visualization using reflective flakes. *J. Fluid Mech.* **152**, 235–248.

SCHREIBER, R. & KELLER, H. B. 1983*a* Spurious solutions in a driven cavity calculations. *J. Comp. Phys.* **49**, 165–172.

SCHREIBER, R. & KELLER, H. B. 1983*b* Driven cavity flows by efficient numerical techniques. *J. Comp. Phys.* **49**, 310–333.

SHEARER, C. J. 1973 Mixing of highly viscous liquids: flow geometries for streamlines subdivision and redistribution. *Chem. Engng. Sci.* **28**, 1091–1098.

SMALE, S. 1963 Diffeomorphisms with many periodic points. In *Differential and Combinational Topology* (ed. S. S. Cairns), pp. 63–68. Princeton University Press.

SMALE, S. 1967 Differentiable dynamical systems. *Bull. Am. Math. Soc.* **73**, 747–817.

TAYLOR, SIR G. I. 1934 The formation of emulsions in definable fields of flow. *Proc. Roy. Soc. Lond.* *A***146**, 501–523.

VAHL DAVIS, G. DE & MALLISON, G. D. 1976 An evaluation of upwind and central difference approximation by a study of recirculating flow. *Comput. Fluids* **4**, 29–46.

WINTERS, K. H. & CLIFFE, K. A. 1979 A finite element study of laminar flows in a square cavity. *UKAERE Harwell Rep.* R9444.